Modelling of cyclic plasticity and crack-tip deformation in a single crystal nickel-based superalloy

B Lin, F Farukh, LG Zhao, A Roy, VV Silberschmidt

Wolfson School of Mechanical and Manufacturing Engineering

Loughborough University, UK

Abstract

In this paper, cyclic plasticity in a single crystal nickel-based superalloy CMSX4 at elevated temperature was modelled using crystal plasticity (CP) and discrete dislocation dynamics (DDD). The CP modelling was carried out at the continuum level based on shear deformation along the octahedral slip systems. The DDD approach was implemented for a representative volume element with periodical boundary conditions. The DDD model parameters were calibrated using the predicted response by the CP model. The obtained numerical results by the two models compared with each other under strain-controlled monotonic and cyclic loading conditions in both <001> and <111> orientations. The CP model was further applied to study crack-tip deformation under fatigue loading. Stress-strain responses, as well as stress and strain distributions, near the crack tip were particularly monitored to assess the role of cyclic plasticity in controlling fatigue-crack propagation. The work has applications in life assessment of nickel-based superalloy components for high-temperature applications.

Keywords: Crystal plasticity; Discrete dislocation dynamics; Representative volume element; Finite element; Cyclic deformation.

1. Introduction

Nickel-based γ/γ' superalloys are commonly used for rotating turbine blades and discs in the hot section of gas turbine engines due to their exceptional high temperature mechanical properties, which are attributed to their characteristic two-phase composite microstructure: a ductile disordered face centred cubic (FCC) Ni-matrix (the γ phase) and coherent $L1_2$-ordered Ni_3Al precipitates (the γ' phase). Most of Nickel-based superalloys have a Ni_3Al phase content that ranges between 40~70%. Nickel-based superalloys are usually exposed to high static or cyclic loads in non-ambient environments, so a reliable prediction of the thermo-mechanical characteristics of the materials is essential for safe life and damage tolerance assessment for fracture critical applications. Therefore, modelling of the mechanical behaviour of Nickel-based superalloys has been the subject of numerous studies.

The mechanical behaviour of engineering alloys can be studied at different scales ranging from atomic (dislocation cores) to macroscopic scale.[1] At grain level, polycrystalline metals possess anisotropic plastic response during deformation due to the random orientation of grain lattices. The physically-based crystal-plasticity theory has been successful for description of anisotropic deformation of single crystals and polycrystals, including body-centered-cubic, face-centered-cubic and highly-closed-packed lattice structures. With the assistance of finite element method, the theory is able to predict the global and local stress-strain response the evolution of crystallographic grain texture and micro-structural crack nucleation in

polycrystalline materials under monotonic, creep and fatigue loading conditions. The inelastic deformation in polycrystalline engineering metallic alloys at room temperature and quasi-static loading rates occurs largely due to dislocation dynamics. Discrete dislocation mechanics (DDD) method[2] has been developed to compute the plastic deformation directly from the evolution of a large number of dislocation segments, particularly in the three-dimensional (3D) dislocation models. The DDD models can explicitly capture the interactions between dislocations on different slip systems, the interactions between dislocations and internal microstructure as well as the formation of different heterogeneous dislocation microstructure such as slip band under both monotonic and cyclic loadings.

Both crystal plasticity theory and DDD method have been employed to investigate the mechanical behaviour of nickel-based superalloys. The crystal plasticity theory has been applied to study creep, fatigue, thermal-mechanical fatigue, indentation deformation and gradient-dependent deformation of single crystal nickel superalloys. Application of the theory has also been extended to model stress-strain response and fatigue crack nucleation for polycrystalline nickel superalloy where microstructure was considered as one of the major factors influencing the fatigue and creep properties of the material. The DDD method has been applied for calculation of yield stress of a nickel-based superalloy, simulation of the cutting of dislocation pairs into the the precipitate phase, prediction of the critical resolved shear stress (CRSS) for precipitate shearing and simulation of the anisotropic mechanical response of a single-crystal nickel-based superalloy.

In this paper, we present CP and DDD models to study cyclic plasticity in a single crystal nickel-based superalloy CMSX4 under monotonic and cyclic loading conditions at 850ºC. The work aims to provide micromechanics based understanding of cyclic deformation behaviour for the material. Furthermore, the CP model was applied to study crack-tip deformation under fatigue loading. Stress-strain responses, as well as stress and strain distributions, near the crack tip were particularly monitored to assess the role of cyclic plasticity in controlling fatigue-crack propagation.

2. Crystal plasticity method

2.1 Crystal plasticity constitutive model

The framework of crystal plasticity theory relies on the multiplicative decomposition of the total deformation gradient $\boldsymbol{F}$ into an elastic ($\boldsymbol{F}^{\mathrm{e}}$) part and a plastic ($\boldsymbol{F}^{\mathrm{p}}$) part:[3]

$$\boldsymbol{F} = \boldsymbol{F}^{e}\boldsymbol{F}^{p} \tag{1}$$

where $\boldsymbol{F}^{\mathrm{e}}$ represents the elastic stretching and rigid-body rotation of the crystal and $\boldsymbol{F}^{p}$ describes crystallographic slip along slip planes due to dislocation motion.

The component $\boldsymbol{F}^{p}$ is calculated from the inelastic velocity gradient:[3]

$$\boldsymbol{L}^{P} = \dot{\boldsymbol{F}}^{P}\boldsymbol{F}^{P^{-1}} = \sum_{\alpha=1}^{n} \dot{\gamma}^{\alpha}(\boldsymbol{m}^{\alpha} \otimes \boldsymbol{n}^{\alpha}) \tag{2}$$

where $\dot{\gamma}^{\alpha}$ is the shear strain rate on the slip system α, $\boldsymbol{m}^{\alpha}$ and $\boldsymbol{n}^{\alpha}$ are the slip direction and the slip plane normal, respectively.

The flow rule is expressed in terms of two scalar state variables per slip system, slip resistance (S^{α}) and back stress (B^{α}):[4]

$$\dot{\gamma}_\alpha = \dot{\gamma}_0 exp\left[\frac{-F_0}{\kappa\theta}\left\langle 1 - \left\langle \frac{|\tau^\alpha - B^\alpha| - S^\alpha \mu/\mu_0}{\hat{\tau}_0 \mu/\mu_0} \right\rangle^p \right\rangle^q \right] sgn(\tau^\alpha - B^\alpha) \quad (3)$$

where κ is the Boltzmann constant, τ^α is the resolved shear stress on the slip system α, θ the absolute temperature, μ and μ_0 the shear moduli at θ and 0 Kelvin, respectively, and F_0, $\hat{\tau}_0$, p, q and $\dot{\gamma}_0$ are material constants. The brackets imply that ⟨x⟩ = x for x > 0 and ⟨x⟩ = 0 for x ≤ 0.

The slip resistance S^α on a generic slip system is assumed to evolve according to the following relation, starting at an initial value of S_o :[5]

$$\dot{S}^\alpha = [h_S - d_D(S^\alpha - S_0^\alpha)]|\dot{\gamma}^\alpha| \quad (4)$$

where the first and second terms are static and dynamic recovery terms associated with the material constants h_S and d_D, respectively.

The back stress B^α evolves according to a standard hardening-dynamic recovery format:[21]

$$\dot{B}^\alpha = h_B \dot{\gamma}^\alpha - r_D B^\alpha |\dot{\gamma}_\alpha| \quad (5)$$

where h_B is a hardening constant, and r_D is a dynamic recovery function which introduces the inherent dependency between the slip resistance and back stress and may be expressed as:[4]

$$r_D = \frac{h_B \mu_0}{S^\alpha}\left\{\frac{\mu_0'}{f_c \lambda} - \mu\right\}^{-1} \quad (6)$$

where f_c is a coupling parameter between the internal slip variables and μ_0' the local slip shear modulus at 0 Kelvin.

The crystallographic formulation was implemented numerically into the finite element (FE) code ABAQUS within the framework of large strain kinematics via a user-defined material subroutine (UMAT), where the fully implicit (Euler backward) integration algorithm was adopted.

2.2 Finite element model

A single 3D element, C3D8 in ABAQUS, was used to model the stress-strain response of CMSX4. The element was subjected to a displacement in the z-direction while constrained in the x and y directions.

A three-point bending specimen with dimensions shown in Fig. 1a was considered for crack tip deformation analysis for both <001> and <111> orientations. The finite element mesh near the crack tip, as shown in Fig. 1b, consists of four-node first-order plane-strain elements with full integration. Two dimensional elements were chosen due to the prevailing plane-strain deformation of the specimen. Cyclic load with a triangular waveform and a frequency of 0.5Hz was applied to the middle node on the bottom side of the specimen (Fig. 1a), which is also constrained in the x-direction to avoid the rigid body motion. While the two supports on the top side of the specimen are constrained in the y-direction The total crack length was chosen to be a = 4 mm, i.e., a/W = 0.4, which includes the notch with a depth of 2.5 mm and a precrack with a length of 1.5 mm. A maximum load of 4 kN with 0.1 load ration was applied at the middle of the bottom surface. This load corresponds to a stress intensity factor (SIF) of ΔK = 31.6 MPa√m, which was verified using analytical solutions. The same level of load was applied to the finite element model in both <001> and <111> orientations.

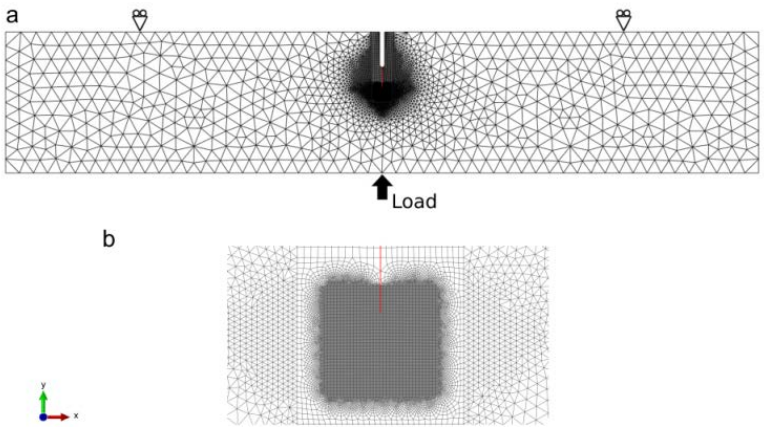

Fig. 1. FE model for crack tip deformation analysis: (a) mesh for the SENB sample; (b) refined mesh near the crack tip

3. Discrete dislocation dynamics method

3.1 Simulation model

A representative volume element (RVE) with periodic boundary condition (PBC), containing a γ′ cubic precipitate and γ channels, was built to represent nickel-based single crystal superalloy – CMSX4 (Fig. 2).

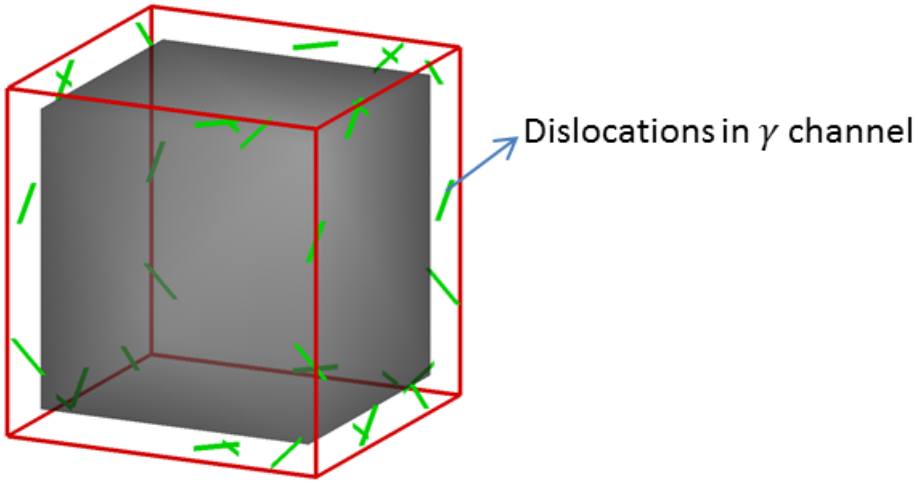

Fig. 2. RVE model with γ′ precipitate and γ matrix.

To simulate the dislocation multiplication, Frank-Read sources with an initial dislocation density were randomly distributed on the 12 octahedral slip systems in the FCC matrix channel. A uniaxial load was applied to the RVE in both the <001> and <111> orientations under strain-controlled condition. Both the γ and γ′ phases were assumed to be isotropic with the same shear modulus *G* and Poisson's ratio *v*. As the PBC condition is applied to the RVE, artificial self-annihilation of dislocation loops occurs. To avoid this, the RVE needs to have a

non-perfect cubic shape. At a channel with d = 95b and a precipitate volume fraction f = 70%, the dimensions of the RVE and the precipitates are 1610b x 1690b x 1770b and 1420b x 1500b x 1580b, respectively.

3.2 Peach-Koehler (PK) force, Equations of motion and Short range reactions

Dislocations are represented by a set of nodes connected to each other by straight segments and the evolution of each dislocation segment is determined by the motion of dislocation nodes. The Peach–Koehler force exerted by the long-range stress (σ^{net}) and the external applied stress (σ^{app}) can be calculated using the Peach–Koehler equation:

$$F_i = (\sigma^{net} + \sigma^{app}) \cdot b_i \times \xi_i \tag{7}$$

where b_i and ξ_i are the Burgers vector and line sense vector of segment *i*, respectively.

For each dislocation segment, the free glide velocity of dislocation v_i^{glide} during a simulation time step may be determined as:

$$v_i^{glide} = \begin{cases} 0 & \text{if } \mathrm{abs}\left(\mathrm{F_i^{glide}}\right) \le \mathrm{abs}(\tau_F b_i) \\ \frac{F_i^{glide}}{B} & \text{if } \mathrm{abs}\left(\mathrm{F_i^{glide}}\right) > \mathrm{abs}(\tau_F b_i) \end{cases} \tag{8}$$

where F_i^{glide} is the glide component of the Peach-Koehler force F_i on the slip plane, τ_F a constant friction stress and B the viscous drag coefficient.

A back force model[6] was introduced to simulate γ' precipitate shearing by a series of superdislocations. The leading and trailing dislocations form a superdislocation, separated by an antiphase boundary (APB). To determine whether the dislocation segment entering into the γ' precipitate is a leading dislocation or a trailing dislocation, the following method is applied in the DDD simulations: If $F_{app} \cdot F_{int} < 0$ and $abs(F_{int}) > 0.25\chi_{APB}$, a trailing dislocation enters the γ' precipitate; If $F_{app} \cdot F_{int} \geq 0$ and $abs(F_{int}) > 0.25\chi_{APB}$, a leading dislocation enters the γ' precipitate. Here, F_{app} and F_{int} are the glide forces induced by the external loads and the stress at the centre of dislocation segment *i*, respectively. χ_{APB} is the inherent APB energy per unit area.

Besides gliding under the PK force, dislocations interact with each other by short-range interactions under mechanical loading. Short-range interactions considered in the DDD model include annihilation and formation of jogs and junctions. A complete list of the short-range interaction rules for dislocation dynamics was given by Rhee et al.[7]

3.3 Dislocation-induced plastic strain and Computation of the external stress

In the DDD model, assuming that the model is subjected to a homogeneous macroscopic stress state, as shown in Fig. 3, a macroscopic plastic strain ε_{ij}^p is produced by:[8]

$$\varepsilon_{ij}^p = \frac{1}{V}\int_{A_{slip}} \frac{1}{2}\left(n_i b_j + n_j b_i\right) dA \tag{9}$$

where b_i is the Burgers vector, dA is the incremental area swept out by the segment, n_i is the normal vector of the glide plane, V is the simulation volume, and A_{slip} is the collection of surfaces active in deformation.

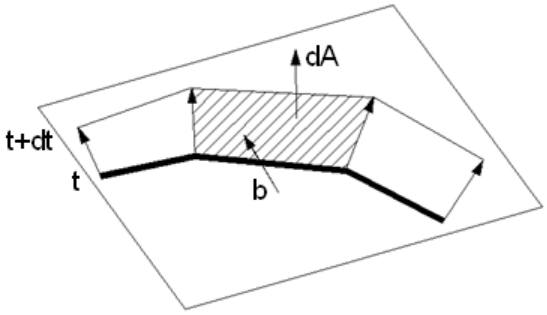

Fig. 3. Plastic strain increment produced by the motion of a single dislocation segment.

If the RVE is loaded along the z-axis at a fixed strain rate $\dot{\varepsilon}$, the total strain ε_z^{tot} along the loading direction should be:

$$\varepsilon_z^{tot} = \dot{\varepsilon} * t \tag{10}$$

By considering equations (9) and (10), we get the elastic strain $\varepsilon_z^e(t)$ is:

$$\varepsilon_z^e(t) = \varepsilon_z^{tot}(t) - \varepsilon_z^p(t) \tag{11}$$

So the time-dependent external stress $\sigma_z^{ext}(t)$ is:

$$\sigma_z^{ext}(t) = E\varepsilon_z^e(t) = E(\varepsilon_z^{tot}(t) - \varepsilon_z^p(t)) \tag{12}$$

where E is the Young's modulus.

4. Numerical results and discussion

4.1 Determination of model parameters

The full model parameters in the CP model are already available at 850ºC for CMSX4 nickel single crystals.[5] Numerical predictions of the monotonic and steady cyclic responses with different strain rates and loading orientations have been presented by Dennis.[5] It was shown that the CP model captured both the strain rate sensitivity and the effects of material orientation very well. Applying the same model parameters, the monotonic and first-cyclic responses of the material are predicted by the CP model at strain rate $\dot{\varepsilon} = 1s^{-1}$ and shown in Figs. 4 and 5.

The model parameters used in the DDD model were calibrated by fitting the monotonic stress-strain curves and the first cyclic loop obtained by the CP model at strain rate $\dot{\varepsilon} = 1s^{-1}$ for the <001> and <111> orientations. Prior to the fitting process, some material constants, such as: APB energy, drag coefficient and initial dislocation density were estimated from the literature.[9] Following each simulation, the resulting stress values were compared with the experimental data. The material constants were ‘‘tuned’’ untill a good match was obtained. The fitted material constants for the DDD model are shown in Table 1.

Table 1

Material parameters in DDD model at 850ºC

Orientation	E (GPa)	G (GPa)	ν	b (nm)	B (Pa s)	τ_F (MPa)	χ_{APB} (mJ/m^2)	Initial dislocation density (m^{-2})
<001>	91.92	103.5	0.379	0.25	8.3e-6	200	162.5	2.5e+13
<111>	244.55	43.06	0.179					

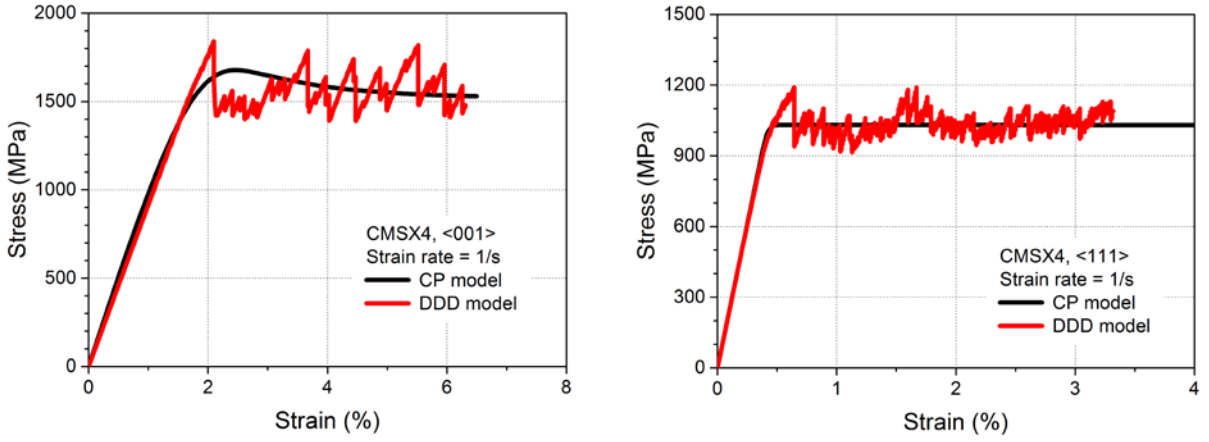

(a) (b)

Fig. 4. Monotonic response by CP and DDD models at $\dot{\varepsilon}$ = 1/s and for: (a) <001>; (b) <111>.

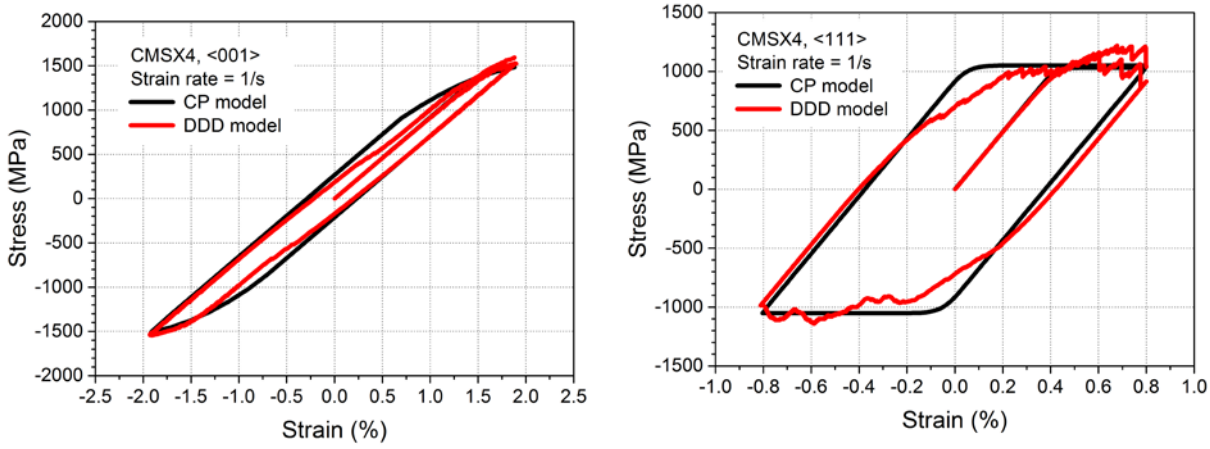

(a) (b)

Fig. 5. Cyclic response by CP and DDD models at $\dot{\varepsilon}$ = 1/s and for: (a) <001>; (b) <111>.

4.2 Stress-strain response by CP and DDD models

The simulated stress-strain response for monotonic and cyclic loading by CP and DDD models are shown in Figs. 4 and 5. Clearly, the predicted stress-strain responses by the two models have a good agreement. It can be seen from the monotonic response in Fig. 4 that three-stage deformation: the initial elastic stage I, the hardening stage II and the softening stage III are observed, but the amount of hardening is shown to be varying with crystal orientation and material constitutive model. Especially, in the CP modelling for <111> orientation, the hardening amount is very limited so the stress-strain behaviour of the material is characterized by elastic-perfectly plastic behaviour. Moreover, the CP model predicts a smoother softening stage than the DDD model. The first cyclic loop for both <001> and <111> orientations are shown in Fig. 5. For the < 001 > orientation, the amount of inelastic deformation is very small, as revealed by the thin hysteresis loop in Fig. 5a. The stress-strain loop (Fig. 5b) is much wider for the <111> orientation than that for the <001> orientation, indicating more inelastic deformation in the material for the <111> orientation. It can also be seen from Figs. 4 and 5 that the monotonic and cyclic responses are strongly dependent on the crystal orientation.

4.3 Modelling of crack-tip deformation

Crack tip deformation was studied by applying cyclic load to the 3-point bend stationary crack model (Fig. 1). A total of five cycles was simulated by considering a triangular loading waveform with a load ratio of R = 0.1, a maximum load of 4kN and a frequency of 0.5Hz. The load corresponds to a stress intensity factor range of $\Delta K = 31.6$ MPa$\sqrt{m}$. Fig. 6 shows the stress distribution near the crack tip in both <001> and <111> direction which exhibits the high orientation dependency of stress-strain behaviour of CMSX4. This is also observed from the normal (in x-direction) stress-strain loops averaged over the element just ahead of the crack tip (see Fig. 7). It is noted that the stress-strain loops in the <111> orientation exhibit more ratchetting than those in the <001> direction.

The stress-strain response at the crack tip were predicted using CP model, without considering the dislocation sources. Simulation based on DDD model, considering the presence of dislocations, was shown to produce higher level of stress concentration near the crack tip as mentioned in Šiška et al.[10] Additionally, it was observed that CP model did not predict accurately the hardening behaviour of the material for the <111> orientation. The analysis of crack tip deformation using DDD will be conducted in our future studies.

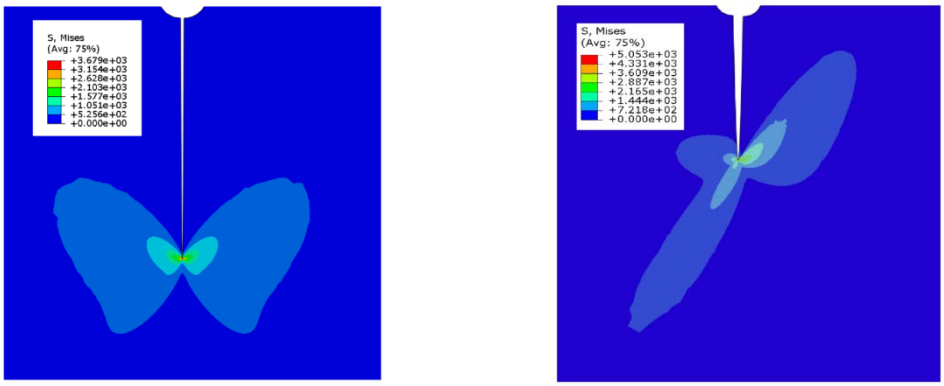

(a) (b)

Fig. 6. Contour plot of Mises stress near the crack tip along (a) <001> and (b) <111> directions for a triangular loading waveform ($\Delta K = 36.1$ MPa$\sqrt{m}$, R = 0.1 and f = 0.25Hz).

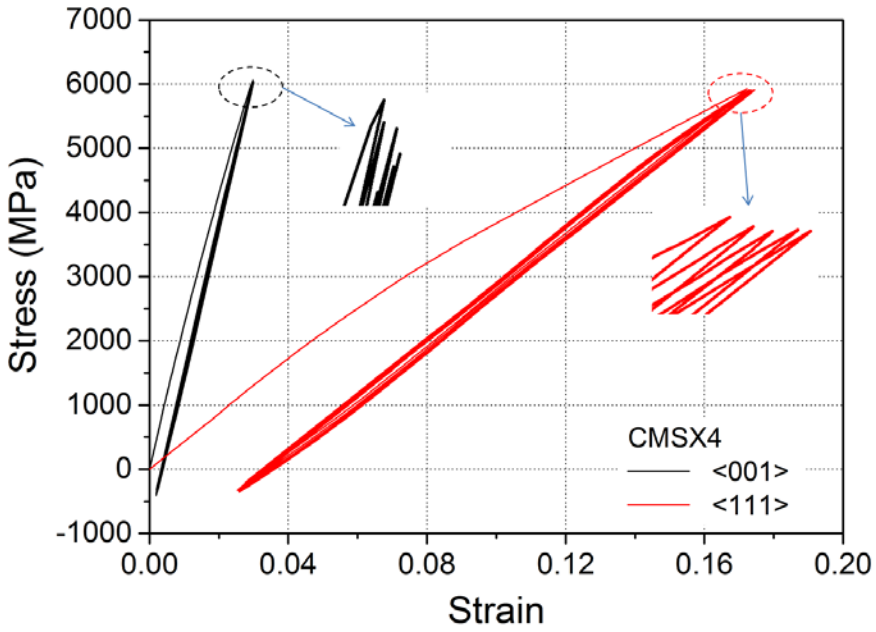

Fig. 7 Stress-strain loops just ahead of the crack tip obtained by the CP model.

5. Conclusions

Both CP and DDD models have been used to simulate macroscopic responses of a single crystal nickel-based superalloy CMSX4 subjected to monotonic and cyclic loadings at elevated temperature, respectively. The predictions of the two micromechanical models have a good agreement with each other in both <001> and <111> orientations and the orientation-dependent stress-strain behaviour of CMSX4 has been well predicted.

The CP model was further applied to study crack-tip deformation under fatigue loading for both <001> and <111> directions, which also confirmed the high orientation dependency of stress-strain behaviour near the crack tip.

Acknowledgements

The work was funded by the EPSRC (Grants EP/K026844/1 and EP/M000966/1) of the UK.

References

[1] D.L. McDowell. Int. J. Plast. 26 (2010) 1280-1309.

[2] H.M. Zbib, T. D. de la Rubia, Int. J. Plast. 18 (2002) 1133-1163.

[3] R.J. Asaro, Adv. Appl. Mech. 23 (1983) 1-115.

[4] E.P. Busso, Cyclic deformation of monocrystalline nickel alluminide and high temperature coatings, Ph.D. Thesis, Massachusetts Institute of Technology, USA, 1990.

[5] R.J. Dennis, Mechanistic modelling of deformation and void growth behaviour in superalloy single crystals, Ph.D. Thesis, Imperial College London, UK, 2000.

[6] K. Yashiro, F. Kurose, Y. Nakashima, K. Kubo, Y. Tomita, H.M. Zbib, Int. J. Plast. 22 (2006) 713-723.

[7] M. Rhee, H.M. Zbib, J.P. Hirth, H. Huang, T.D. de La Rubia, T.D., Model. Simul. Mater. Sci. Eng. 6 (1998) 467-492.

[8] J.R. Rice, J. Appl. Mech. 37 (1970) 728-737.

[9] S. Gao, M. Fivel, A. Ma, A. Hartmaier, J. Mech. Phys. Solids 76 (2015) 276-290.

[10] F. Šiška, D. Weygand, S. Forest, P. Gumbsch, Comput. Mater. Sci. 45 (2009) 793–799.